PFHydro: A New Watershed-Scale Model for Post-Fire Runoff Simulation

Jun Wang [a,*], Michelle A. Stern [b], Vanessa M. King [a], Charles N. Alpers [b], Nigel W.T. Quinn [c], Alan L. Flint [b], Lorraine E. Flint [b]

[a] U.S. Bureau of Reclamation, Sacramento, CA, USA
[b] California Water Science Center, U.S. Geological Survey, Sacramento, CA, USA
[c] Berkeley National Laboratory, Berkeley, CA, USA

A B S T R A C T

Runoff increases after wildfires that burn vegetation and create a condition of soil-water repellence (SWR). A new post-fire watershed hydrological model, PFHydro, was created to explicitly simulate vegetation interception and SWR effects for four burn severity categories: high, medium, low severity and unburned. The model was applied to simulate post-fire runoff from the Upper Cache Creek Watershed in California, USA. Nash–Sutcliffe modeling efficiency (NSE) was used to assess model performance. The NSE was 0.80 and 0.88 for pre-fire water years (WY) 2000 and 2015, respectively. NSE was 0.88 and 0.93 for WYs 2016 (first year post-fire) and 2017 respectively. The simulated percentage of surface runoff in total runoff of WY 2016 was about six times that of pre-fire WY 2000 and three times that of WY 2015. The modeling results suggest that SWR is an important factor for post-fire runoff generation. The model was successful at simulating SWR behavior.

1. Introduction

In addition to the immediate threat posed by wildfires, such events can also threaten natural resource sustainability by increasing runoff and erosion in the years following a fire. Increased post-fire surface runoff is directly associated with increased erosion and mud flow.

Experimental plot and hillslope-scale studies indicate that wildfires may increase rainfall-event-induced runoff and soil erosion by a factor of 2–40 on small-plot scales and by more than 100-fold on large-plot to hillslope scales (Williams et al., 2014). In burned areas, annual sus-pended sediment yields can increase by a factor of between 1 and 1459 as compared with suspended sediment yields under unburned condi-tions (Smith et al., 2011). For example, sedimentation from flooding after the 1996 Buffalo Creek Fire in Colorado reduced Denver's municipal reservoir capacity by roughly a third (Agnew et al., 1997).The Thomas Fire of southern California (December 4, 2017–January 12, 2018), which burned 1141 square kilometers (km^2), was followed by heavy rains that led to mudflows and 21 deaths in the unincorporated community of Montecito in Santa Barbara County, California (Dolan, 2018).

The runoff response from burned watersheds is a function of rainfall amount and intensity, burn severity, and properties of the impacted soils and vegetation cover (Moody and Martin, 2001; Benavides-Solorio and MacDonald, 2005; Spigel and Robichaud, 2007). The reduction of vegetation cover may reduce interception, thereby reducing moisture storage, increasing water yields, and creating greater runoff with smaller storms, while the elimination of transpiration increases soil moisture and streamflow (Neary et al., 2003). The first-order effect of fire on runoff and erosion is decreased interception. Unburned shrubs and co-nifers can intercept up to 35% of rainfall during high intensity storms and 80% of rainfall during low intensity storms (Rowe, 1948; Hamilton and Rowe, 1949 ; Skau, 1964; Tromble, 1983;Owens et al., 2006). Rainfall interception by rangeland plants can reduce erosivity of high-intensity rainfall by up to 50% (Wainwright et al., 1999; Martinez-Mena et al., 2000). Numerous studies in forested areas have found rainfall erosivity and its dissipation by vegetation cover to be the primary factors controlling post-fire erosion rates (Inbar et al., 1998; Moody and Martin, 2001, 2009; Benavides-Solorio and MacDonald, 2005; Spigel and Robichaud, 2007; Robichaud et al., 2008, 2013a, 2013b).

In addition to changes in rainfall interception, wildfire can cause the alteration of soil physical and chemical properties that can impact soil structure and increase soil-water repellence (SWR) for a significant period of time. Numerous watershed-scale studies considered fire- induced SWR to be a major factor controlling post-fire runoff and erosion rates (Morris and Moses, 1987; Imeson et al., 1992; Shakesby

* Corresponding author.
E-mail address: junwang@usbr.gov (J. Wang).

et al., 2000; Letey, 2001). Post-wildfire infiltration into the unsaturated zone is controlled by fire-induced changes in soil-water storage and soil hydraulic properties. After a fire, water repellency is typically found as a discrete layer of variable thickness and spatial continuity found on the soil surface or a few centimeters below and parallel to the mineral soil surface. Water repellency has been shown to be created and intensified by soil heating that occurred during a fire (DeBano, 1966; DeBano and Krammes, 1966). This soil condition dramatically reduces infiltration, increases overland flow, and consequently amplifies the risk of severe erosion. Increased SWR and reduced vegetation interception/protection are major causes of increased post-fire overland flow and erosion. Under field conditions, the water-repellent soil layer is not typically contin-uous, so irregular wetting patterns are common (Bond, 1964; Meeuwig, 1971; DeBano, 1981; Dekker and Ritsema, 1995). An increase in bare ground post-fire increases the connectivity of water-repellent soil patches (Shakesby et al., 2000; Doerr and Moody, 2004; Cawson et al., 2010; Nyman et al., 2010). A possible threshold of 60–70% bare ground was found to be related to the connectivity of the bare patches (Johansen et al., 2001) and seemed to explain much of the post-wildfire erosion caused by increased runoff (Moody et al., 2013). Another commonly observed phenomenon is that SWR decreases with increasing soil moisture (MacDonald and Huffman, 2004). Once wet, soils are no longer water repellent until they become desiccated (Doerr and Thomas, 2000). For unburned soils, soil moisture thresholds that mark the range of soil infiltration properties from hydrophobic to hydrophilic occur between 2 and 5% moisture for a dune sand (Dekker et al., 2001), 5–12% moisture for naturally hydrophobic soils (de Jonge et al., 1999), and 34–38% moisture for clayey peat soils (Dekker and Ritsema, 1995). There are very few data that can be used to suggest a soil moisture threshold for the elimination of SWR; however, Doerr and Thomas (2000) noted an absence of SWR once the soil moisture content exceeded 28% in a coarse-textured forest soil in Portugal. Huffman et al. (2001) reported that the soil moisture threshold ranged from about 12% in unburned areas to above 25% in severely burned areas in experiments conducted in the Colorado Front Range. A study by MacDonald and Huffman (2004) suggested that the soil moisture threshold for the shift from hydrophobic to hydrophilic soil properties was about 10% for unburned sites, 13% for sites burned at low severity, and 28% for sites burned at moderate severity.

Depending on the post-fire response domain, hillslope-runoff- generating processes may be described by either of two conceptual models of runoff generation, or a combination of both: infiltration- excess or saturation-excess overland flow (Dunne, 1978; Wondzell and King, 2003; Keizer et al., 2005; Onda et al., 2008; Ebel et al., 2012). Under the former model, the runoff volume is limited by the infiltration capacity of the soil. Under the latter model, the saturation state of the soil limits any further infiltration. The relative weight of the two runoff-generating processes can vary on steep hillslopes between suc-cessive rainfall events (Schmidt et al., 2011). Post-fire, both runoff-generating mechanisms can occur within the same watershed. In humid areas, saturation-excess runoff processes typically dominate under pre-fire conditions, whereas infiltration-excess runoff processes are expected to dominate in burned areas during the first 1–2 years post-fire while SWR effects remain.

For the above reasons, a realistic post-fire, watershed-scale runoff model should simulate the following: (a) both infiltration-excess and saturation-excess overland flow; (b) vegetation precipitation intercep-tion for pre- and post-fire conditions; and (c) post-fire soil water repel-lent behavior. In this paper, we introduce PFHydro, a new watershed- scale post-fire runoff model that simulates those three phenomena and demonstrate its application to the Upper Cache Creek Watershed in northern California, USA.

1.1. Review of post-fire rainfall-runoff simulation models

There are several existing public-domain and proprietary models that are used to simulate post-fire effects on rainfall-runoff generation. Much of the hydrological research literature has focused on predicting peak discharge of post-fire runoff by using the paleo-flood method (e.g. Jarrett and England, 2002), the curve number method (Hawkins and Greenberg, 1990; Cerrelli, 2005; Foltz et al., 2009), or direct measure-ments from burned basins (Moody and Martin, 2001; Moody et al., 2008; Foltz et al., 2009; Kean et al., 2011; Moody, 2012). Little research has covered predicting flood timing relative to rainfall (Elliot et al., 2010).

Early models utilized the rational method to compute total discharge ($Q = CIA$, where C is runoff coefficient, I is rainfall intensity, and A is contributing area), which was designed to calculate the flood peak flow under the assumption that the intensities of both rainfall and infiltration were uniformly distributed in time and space (Ponce, 1989). However, curve number methods have difficulties accounting for fire effects (Moody et al., 2013). For post-fire hydrology simulation, Moody et al. (2008) developed a new burn severity variable known as the hydraulic functional connectivity (Φ), which incorporates both the magnitude of the burn severity and the spatial sequence of the burn severity along hillslope flow paths. The runoff coefficient C became a linear function of the mean hydraulic functional connectivity of the subwatersheds. The dimensionless hydraulic functional connectivity Φ was computed as follows:

$$\varphi_i = \frac{1}{\alpha} \sum_{i=1}^{k} \alpha_{ij} \Delta NBR_{ij} S_{ij} \quad (1)$$

where α_{ij} is a weighting factor equal to the uphill contributing area to pixel i in flow path j, S_{ij} is the local slope from pixel i to the next downstream pixel in flow path j, α is the total area of the flow path, and the differenced Normalized Burn Ratio (NBR), $\Delta NBR = NBR_{prefire} - NBR_{postfire}$. The total discharge per unit area from a subwatershed could then be represented by the sum of the Φ_i values for each flow path normalized by the number of flow paths.

Luce (2001) developed the Fire Enhanced Runoff and Gully Initiation (FERGI) model, a physically based mathematical description of hillslope hydrologic and geomorphic response for a given set of weather events. FERGI estimated the probability of post-fire rainfall excess, the quantity of runoff generated, and the initiation of gully erosion on hillslopes with and without mitigations using contour-felled logs or log erosion barriers.

A significant advance in physically based, numerical process models for simulating runoff and erosion from simple hillslopes or watersheds came with the introduction of the Water Erosion Prediction Project (WEPP) model (Flanagan et al., 1995). The GIS-based GeoWEPP version of the model (GeoWEPP ArcX, 2003; Renschler, 2003), which utilizes ArcGIS software, combines the WEPP v2002.7 model (Flanagan et al., 1995) with Topography Parameterization software (TOPAZ) (Garbrecht and Martz, 1997) to predict runoff and erosion at the hillslope and watershed scale. GeoWEPP was developed to allow WEPP hillslope parameterization to be based on digital data sources, such as digital elevation models (DEMs), and for digital outputs to be viewed and analyzed in a GIS environment (Renschler, 2003). An online GIS inter-face for the WEPP watershed model was developed to help input spatial files for forested applications including the impacts of wildfire (Frank-enberger et al., 2011). This simplifies downloading or pre-processing of topographic, soils, or land cover databases necessary for running the GeoWEPP model (Miller et al., 2015). WEPP and GeoWEPP were also applied to simulate post-fire runoff and soil erosion (Elliot et al., 2006; Miller et al., 2016). The soil burn severity map was an input for WEPP and GeoWEPP simulations to help to quantify burn effects on soils runoff and erosion.

Kinoshita et al. (2014) reviewed five models for post-fire peak discharge predictions: the Rowe Countryman and Storey (RCS) (Rowe et al., 1949), United States Geological Survey (USGS) Linear Regression Equations (Foltz et al., 2009), USDA Windows Technical Release 55 (TR_55) (USDA, 2009), Wildcat5 (Hawkins and Munoz, 2011), and U.S. Army Corps of Engineers (USACE) Hydrologic Modeling System

(HEC-HMS) (USACE, 2010). The TR_55, HEC-HMS and Wildcat5 were curve number-based models. These models were applied to eight diverse basins in the western United States affected by wildfires. According to Kinoshita et al. (2014), no one model performed sufficiently well for application to all study sites. The review results showed inconsistency between model predictions for events across the sites and poor results with larger return periods (25- and 50-year events) and when applied to post-fire watershed simulations.

Chen et al. (2013) evaluated the capability of four models repre-senting empirical, semi-empirical, and process-oriented methods for simulation of post-fire hydrology using data from the San Dimas Experimental Forest (SDEF), San Dimas, California. The four models are: empirical-based Rule of Thumb by Kuyumjian (Foltz et al., 2008) and Rational Method (MODRAT) (LACDPW, 1991), semi-empirical HEC-HMS, and physical, process-oriented KINematic Runoff and EROSion Model 2 (KINEROS2) (Goodrich et al., 2005). These modeling studies showed that simple, empirical peak flow models may perform acceptably if calibrated correctly. However, these models may not be applicable for watersheds outside the area where they were calibrated when they do not incorporate pertinent hydrological mechanisms. Analysis by Chen et al. (2013) suggests that the runoff-generation mechanism in the watershed may have changed from a saturation-excess runoff to an infiltration-excess dominated runoff mechanism due to fire effects. Physically based, process-oriented models can be valuable for in-depth analysis of pre- and post-fire hydrographs and provide consistent and satisfactory predictions (Chen et al., 2013).

In summary, most hydrological models simulating post-fire runoff are event-based for peak discharge using curve-number or regression methods. The curve-number-based models are best applied to small watersheds where infiltration-excess mechanism dominates. Regression- method-based models are limited to use in watersheds with similar characteristics to the watershed for which the regression equations were developed. However, burn severity, which represents the post-fire im-pacts on vegetation and soil characteristics and subsequent rainfall runoff response, needs to be incorporated into this modeling approach. The physically based WEPP/GeoWEPP model that incorporates burn severity has been applied in some watersheds to simulate post-fire runoff and soil erosion in a hillslope and watershed scale. However, this and other models are limited in their capability to simulate post-fire runoff when vegetation cover and soil properties change, due to changes in factors such as vegetation interception, evapotranspiration, and water repellency. A physically based model is needed that can quantify post- fire changes in vegetation interception and water repellency and has both saturation-excess and infiltration-excess runoff generation mech-anisms to improve simulation of wildfire effects on runoff generation and subsequent soil erosion on a watershed scale.

2. Methods to the development of a new post-fire hydrologic model

A new watershed scale post-fire hydrologic model, PFHydro, was created based on UFORE-Hydro (Wang et al., 2005, 2008) by integrating algorithms to quantify SWR effects and modifying the model structure to simulate rainfall runoff in both unburned areas and burned areas with four burn severity categories. UFORE-Hydro (now called i-tree hydro), which is based on TOPMODEL theory (Beven and Kirkby, 1979; Beven, 1997a, 1997b; Kirkby, 1997), can simulate rainfall runoff process in a watershed scale (snowmelt component is under development).

2.1. A summary of UFORE-Hydro and TOPMODEL theory

TOPMODEL has been used for numerous watershed hydrologic simulation applications. TOPMODEL is a semi-distributed hydrological model that assumes that watershed topography exerts control of flow routing through upland catchments. The model allows variable contributing area and catchment topography and allows for variable soil transmissivity with soil depth to improve the simulation of watershed runoff. The original TOPMODEL was applied to catchments with shallow soils and moderate topography, which typically do not experience extended dry periods. Saturation-excess overland flow processes are likely to dominate in this type of catchment. A later version of TOP-MODEL (Beven, 1984) used the exponential Green-Ampt model to calculate infiltration-excess runoff. A major advantage of TOPMODEL is its simplicity, which is exemplified by the use of the topographic index, *TI* ¼ ln(a/tanβ), where a is the upslope contributing area per unit con-tour length and tanβ represents the local slope. *TI* is used as an index of hydrological similarity. All points with the same index value are assumed to respond in a hydrologically similar way. Hence, it is only necessary to make calculations for points with different index values, spanning the index distribution function for a catchment.

Enhancements to the standard TOPMODEL code were made to create the UFORE-Hydro model (Wang et al., 2005, 2008), a more flexible tool for simulating pre-wildfire hydrologic events. The specific enhance-ments include: (a) a soil topographic index; (b) a power function for the decay of transmissivity with soil depth; and (c) a vegetation interception routine. The Topographic Index approach recognizes that the saturated surface transmissivity $T(z)$ of the soil varies widely over the area of the catchment. The topographic index *TI* ¼ ln(a/tanβ), for each point in the catchment was replaced by a soil topographic index *STI* ¼ ln(a/T_0tanβ), where T_0 is the saturated surface soil transmissivity for each cell. This addition provides model flexibility and allows the model to deal with catchment heterogeneity more readily. Users are required to provide an initial T_0 value for each cell or provide T_0 for several blocks of cells representing different soil types.

To simulate the decline of transmissivity with soil depth, TOPMODEL uses an exponential function $T(z)$ ¼ T_0Exp$(-S_i/m)$ that results in the indices *TI* and *STI*, as defined above. In this formula, T_0 is the trans-missivity at saturation, S_i is the local saturation deficit, and m is a scaling parameter. Beven (1984) demonstrated that this profile signature was not universal, however it was appropriate for many soil profile hydraulic conductivity data sets. A generalized power function decay term, $T(z)$ ¼ T_0 $(1 - S_i/m)^n$ (Ambroise et al., 1996; Iorgulescu and Musy, 1998), was incorporated into the UFORE-Hydro model to help represent the soil infiltration characteristics of different soil types. The user can select a value of n for a particular simulation, which provides flexibility in modeling runoff hydrograph recession characteristics, particularly when soil transmissivity varies with depth and complicates soil infiltration estimation. For exponential decay of soil transmissivity and estimated infiltration, the Topographic and Soil Topographic indices take the following forms:

Topographic index: *TI* ¼ ln (a/tanβ); Soil topographic index: *STI* ¼ ln (a/T_0tanβ)

For those infiltration events that follow a generalized power function decay pattern for soil transmissivity and estimated infiltration, the index is modified as follows:

Topographic index: *TI* ¼ $(a/\tan\beta)^{1/n}$; Soil topographic index: *STI* ¼ $(a/T_0 \tan\beta)^{1/n}$

2.1.1. Simulation of subsurface flow

An important next step in model development involves calculating subsurface flow based on estimates of soil infiltration. For homogenous watersheds using the topographic index where soil hydraulic conduc-tivity decays with soil depth exponentially, the resultant equation for subsurface flow [L/T] is:

$q_{subsurface}$ ¼ $T_0 e^{-\lambda} e^{-\frac{\bar{s}}{m}}$ (2)

where λ ¼ 1=A R lnða =tan βÞdA is the average topographic index, A is contributing area, and $\bar{s}$¼-$m$ln(R/T_0)-$m\lambda$ is the average soil moisture deficit under λ.

Watershed soils are rarely homogeneous, hence when using the soil topographic index for heterogenous conditions, the equation for sub-surface flow becomes:

$$q_{\text{subsurface}} = e^{-\lambda} e^{-\frac{\bar{s}}{m}} \quad (3)$$

where $\lambda = \frac{1}{A}\int_R \ln(a/T_0 \tan\beta)\,dA$ is the average soil topographic index, and $\bar{s} = -m\ln R - m\lambda$ is the average soil moisture deficit under λ.

The generalized power function decay of mean subsurface flow using the topographic index in the case where soil hydraulic conductivity decays with soil depth in a power function profile and where the watershed is homogenous is given as:

$$q_{\text{subsurface}} = T_0 \lambda^{-n} \left(1 - \frac{\bar{s}}{m}\right)^n \quad (4)$$

where $\lambda = \frac{1}{A}\int_R (a/\tan\beta)^{\frac{1}{n}}\,dA$ is the average topographic index, and $\bar{s} = -m[1-(R/T_0)^{1/n}\lambda]$ is the average soil moisture deficit under topographic index λ.

For a heterogeneous watershed using the same soil topographic index and assuming soil hydraulic conductivity decay with depth in a power function profile, the mean subsurface flow can be estimated using:

$$q_{\text{subsurface}} = \lambda^{-n} \left(1 - \frac{\bar{s}}{m}\right)^n \quad (5)$$

where $\lambda = \frac{1}{A}\int_R (a/T_0 \tan\beta)^{\frac{1}{n}}\,dA$ is the average soil topographic index, and $\bar{s} = -m[1-R^{1/n}\lambda]$ is the average soil moisture deficit under λ.

2.1.2. Simulation of saturation excess and infiltration excess overland flow

A major conceptual model improvement in the simulation of rainfall-induced runoff has been the recognition of two main mechanisms of soil infiltration that affect overland flow. The saturation-excess overland flow algorithm considers the moisture status of the soil during a pre-cipitation event. The overland flow rate, $q_{overland}$ *[L/T],* is calculated as a function of the rainfall throughfall and the moisture status (degree of saturation) of the hillslope area as follows:

$$q_{\text{overland}} = \frac{A_{sat}}{A} P \quad (6)$$

where (A_{sat}/A) is the fraction of the hillslope area that is saturated, and P [L/T] is the throughfall.

The infiltration-excess overland flow conceptual model, on the other hand, is represented by an infiltration rate, i, defined by Beven (1984) as follows:

$$i = \frac{dI}{dt} = \frac{\Delta\psi}{\int_{z=0}^{z=Z} \frac{dz}{K_z}} \quad (7)$$

where I is the cumulative infiltration [L], K_z is the hydraulic conduc-tivity at soil depth z, and $\Delta\psi$ is the effective wetting front suction. Two independent algorithms were developed to account for different decay rates of infiltration with depth in the soil profile:

For exponential decay: $K_z = K_0 e^{-fz}$ (8)

For power function decay: $K_z = K_0(1 - fz)^p$ (9)

where f is a scaling parameter. In general, the saturation-excess overland flow mechanism is most often applied to forested areas where rapid infiltration into shallow forest soils produces vadose zone saturation that acts to initiate soil runoff. The infiltration-excess overland flow mech-anism is more applicable to arid areas and post-fire applications where the top soil layers with SWR are the major limitation to infiltration of precipitation and typically leads to an earlier onset of overland flow.

2.1.3. Simulation of vegetation interception

In watersheds subject to wildfire, the presence of vegetation before a fire and the removal of vegetation as a result of the fire can have a significant effect on rainfall interception and erosivity. The UFORE- Hydro vegetation interception routine (Wang et al., 2008) maintains a continuous water balance of rainfall canopy interception and directs a portion of the intercepted flow along the vegetative stem (plant branches and trunk) in a similar manner to the algorithm developed by Rutter (Rutter et al., 1971, 1975). This algorithm also accounts for the effect of precipitation intensity, duration and changing vegetation cover on both rainfall throughfall and canopy interception according to the expression:

$$\frac{\Delta C}{\Delta t} = P - R - E \quad (10)$$

where C (m) is the depth of water on the unit canopy at time t, P (m/s) is above-canopy precipitation rate, R (m/s) is the below-canopy throughfall precipitation rate that reaches the ground (reduced from total P by canopy interception), E (m/s) is the evaporation rate from the wet can-opy, and $\Delta t$is the simulation time interval (s in this example).

This model allows a small amount of precipitation to fall through the canopy as free throughfall (P_f) without contact with vegetation, and allows interception to increase to a threshold $C_{\max}$, which is the maximum water retained on the canopy. In this case R is equal to P_f. In the UFORE-Hydro model the value of P_f was selected to be comple-mentary to the canopy cover fraction, c, which is related to the canopy leaf area index (LAI) and is relative to the fraction of watershed with vegetation cover following van Dijk and Bruijnzeel (2001). Canopy leaf storage, S, is defined as the water retained on the canopy that would not drain to the ground under normal conditions. This results in the following set of equations:

$$P_f = P(1 - c) \quad (11)$$

$$c = 1 - e^{-\kappa LAI} \quad (12)$$

$$S = S_L LAI \quad (13)$$

where κ is an extinction coefficient and S_L (m) denotes specific leaf storage. The effective vegetation coverage of a watershed is reduced post-fire. The total amount of precipitation that reaches the ground is increased in direct proportion to the burn area and contributes to increased runoff and overland flow.

2.2. Simulating SWR effects in burned areas

As might be expected, the most severe fires typically have the greatest impact on the infiltration characteristics of forest, woodland, and grassland soils. Fire severity affects saturated hydraulic conductiv-ity (K_{sat}) due to factors that change water repellency, including sealing of macropores and combustion of organic matter in near-surface soil layers within the profile (Neary, 2011). High water repellency can reduce K_{sat} to low values or even zero (DeBano et al., 1998; Neary et al., 2005). For a typical high-severity burn, hydrophobic or water-repellent soil conditions can cause a temporary 10–40% reduction in the K_{sat} values in comparison with a normal infiltrating soil (Robichaud, 2000). Blake et al. (2009) noted K_{sat} reductions of 88–92% with high severity wildfire. Saturated hydraulic conductivity reductions of 20–48% are commonly reported (Neary, 2011).

Hence, in the new PFHydro model, the saturated hydraulic conduc-tivity of watershed soils is assigned based on burn severities (unburned, low severity burn, medium severity burn, and high severity burn). The saturated hydraulic conductivities of burned areas can be assigned relative to the unburned saturated hydraulic conductivity K_{sat}, as follows:

1. High severity: μK_{sat}
2. Medium severity: $1.2\mu K_{sat}$
3. Low severity: $1.4\mu K_{sat}$

Where μ is a calibration parameter with values between 0.1 and 0.7 that assumes K_{sat} reductions of 30%–90% with high severity burn. Here K_{sat} is equivalent to K_0 in equations (8) and (9).

There is no known previous research on the relationship between K_{sat} of different burn severities. For PFHydro, the saturated hydraulic conductivity of the low-severity burn area was set to $1.4\mu Ksat$ to ensure its value is lower than the saturated hydraulic conductivity of the un-burned area for the range of μ between 0.1 and 0.7. The saturated hy-draulic conductivity for the medium-severity burn area was then set to $1.2\mu Ksat$, the midpoint between the values for high- and low-severity areas.

The SWR connectivity Φ is a calibration parameter in the PFHydro model with a value between 0 and 1 that represents the fraction of runoff from the burned soils that can be routed to the channel network without further infiltration into the surrounding surface soil.

The SWR significantly decreases with increased surface soil moisture (MacDonald and Huffman, 2004). Researchers have documented persistence of SWR effects from weeks to years (DeBano et al., 1967; Holzhey, 1969). In general, SWR-induced hydrophobicity is broken up, or is sufficiently washed away, within one to two years after a fire (Ritsema and Dekker, 2003). The PFHydro post-fire runoff model makes a simplifying assumption that SWR effects decreased the 2nd year compared to 1st year post-fire, but the effects remain constant within each one-year period post-fire.

3. Modeling application area

One of the major challenges in developing watershed hydrologic and water quality models applicable to wildfire impacts is the difficulty in obtaining appropriate time-series data given the remoteness of the terrain being analyzed and the high cost of obtaining a comprehensive data set. Many watersheds in California have been affected by major wildfire events in recent years, and major fires appear to have become more severe and more costly in terms of lives lost and property damage over the recent decades (Westerling et al., 2014). The Upper Cache Creek Watershed covers portions of Lake County, Yolo County, and Colusa County in northern California (Fig. 1). It has an area of 3,017 square kilometers (km^2), with elevations ranging from approximately 0 to 1,800 m and a total population of about 58,000 (Sacramento River Watershed Program, 2018). This region does not experience significant amounts of snowfall.

During July–August 2015, the Jerusalem and Rocky fires burned a combined 384 km^2 and about 214 km^2 within the Upper Cache Creek watershed downstream of Clear Lake (Fig. 2). The fires varied in in-tensity across the watershed, resulting in spatially variable changes of soil properties and reductions in vegetation cover. A gauged sub area of the Upper Cache Creek Watershed was chosen for the model application area, comprising 282 km^2 in which 163 km^2 were burned. The Shuttle Radar Topography Mission (SRTM) 1-arcsecond digital elevation model (DEM) (USGS, 2014) was reprojected into the State Plane California II coordinate system using ArcGIS and then resampled to a grid size of 30 m for input into the UFORE-Hydro model for pre-fire hydrological simulations and PFHydro model for post-fire hydrological simulations.

3.1. Model vegetation burn estimation

The Rocky and Jerusalem Fire events occurred during the 2015 fire season. The Rocky Fire burned from July 29 to August 14, 2015 and the Jerusalem Fire burned from August 9 to August 25, 2015. The two fires merged on August 12, 2015. Burn severity data for the fires used the Burned Area Reflectance Classification (BARC), a satellite-derived layer of post-fire vegetation conditions. BARC classifies data into four burn

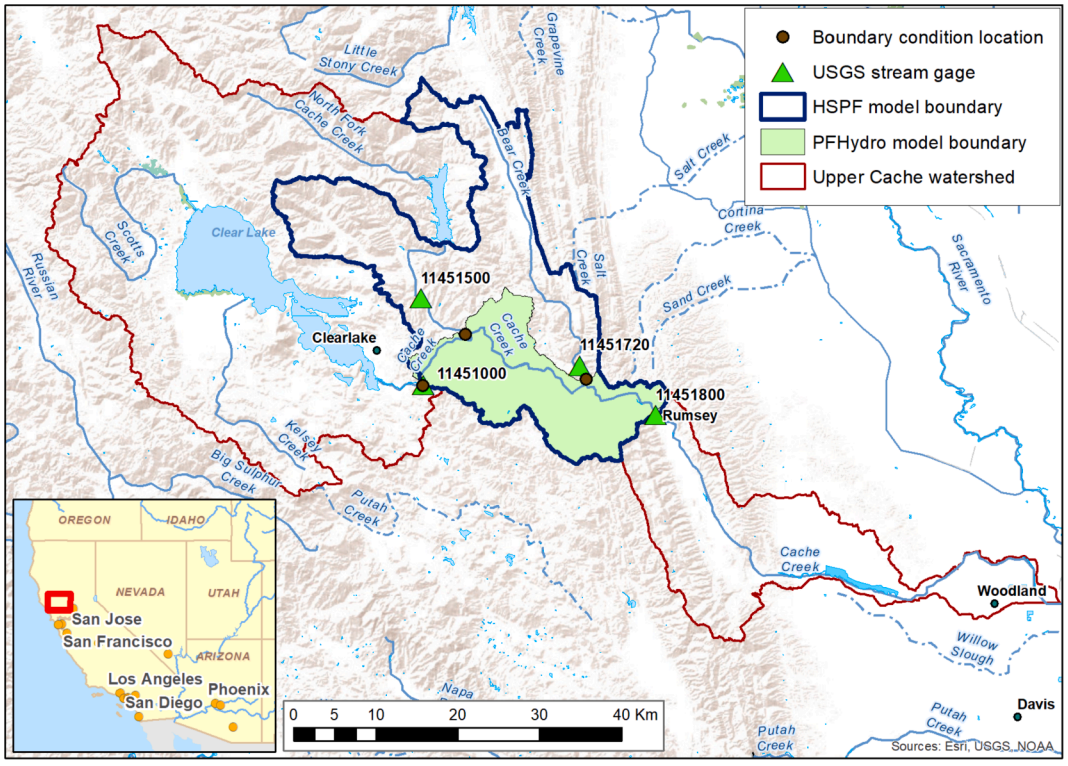

Fig. 1. Location of Upper Cache Creek Watershed in northern California showing boundaries for the HSPF model and PFHydro model. The UFORE-Hydro model boundary is equivalent to the PFHydro model boundary. The map also shows flow monitoring stations located along Cache Creek with outflow from the study watershed at the Rumsey gauge (green triangles), along with locations for hourly time series flow from the HSPF model used as boundary conditions for the PFHydro model (see Section 4.4).

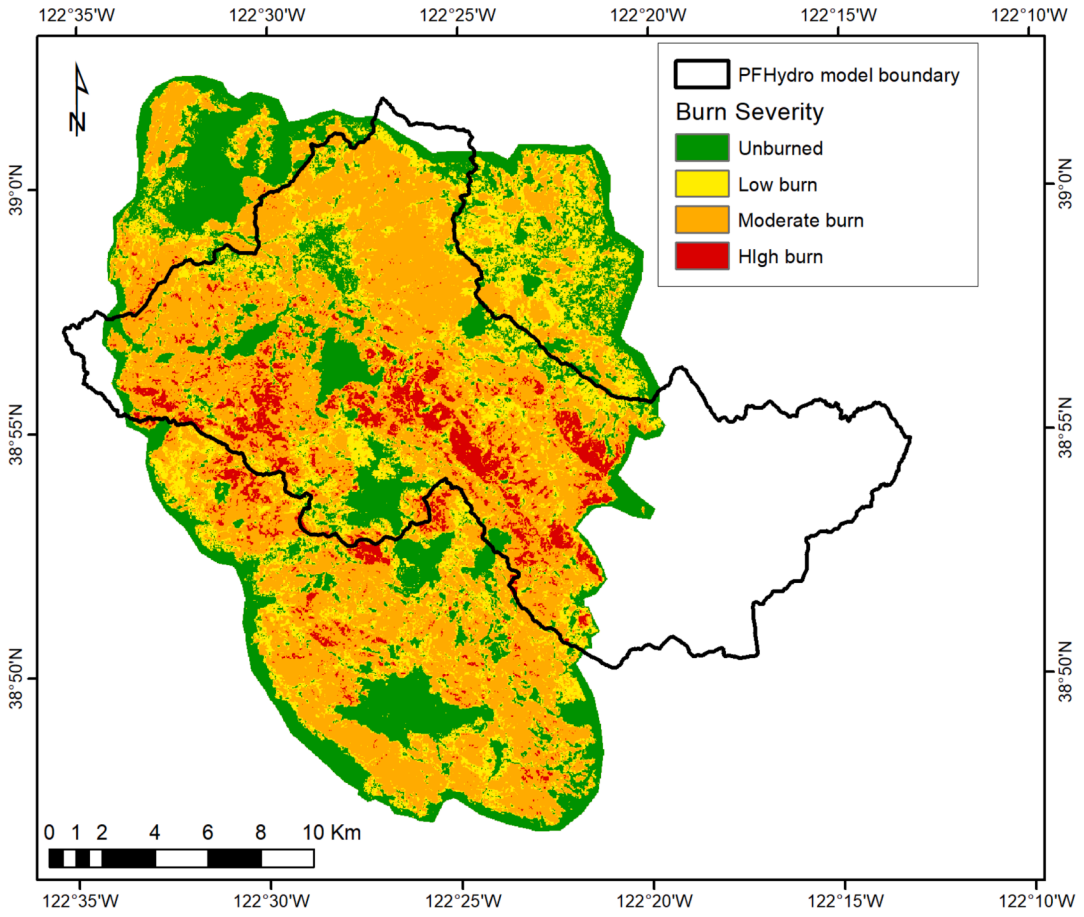

Fig. 2. Burn severity classifications for combined Rocky and Jerusalem Fires. The model application area boundary is shown for reference on the map in the area outlined in black.

severity classes: high, moderate, low, and unburned, based on the relationship between near- and mid-infrared reflectance values (USFS Geospatial Technology and Applications Center, 2018).

The Rocky and Jerusalem Fires were considered a single fire for modeling purposes and the burn severity classification areas were merged accordingly. Fig. 2 shows the burn severity classifications for the combined Rocky and Jerusalem Fires, with the model boundary shown for reference. The areas and percentages of each burn severity class within the model boundary are shown in Table 1.

The percentages of trees and short vegetation pre- and post-fire are used as inputs to PFHydro, in order to calculate the effects of vegetation interception. Two Landsat 8 images were selected for land-cover classification, namely: a pre-fire image taken on July 27, 2015, and a post- fire image taken on September 4, 2015. These images were selected because of their temporal proximity to the start and end dates, respec-tively, of the Rocky and Jerusalem fires, and their lack of visible cloud cover.

Supervised land-cover classification was performed in ArcGIS Pro. The study area contains numerous areas where trees and low vegetation are mixed on scales smaller than the imagery's 30-m pixel size. To account for this, two additional classes were created: one for mixed trees and shrubs, and one for mixed trees and grass. The mixed trees and shrubs class was estimated by visual inspection to contain approximately 50% trees and 50% low vegetation, while the mixed trees and grass class was estimated to contain approximately 30% trees and 70% low vegetation. After classification (Fig. 3), the areas in these classes were split into trees and low vegetation using these percentages to obtain the areas in each of the final five classes listed above and for each burn severity classification (Table 2). The data in Table 2 were input into the PFHydro model for post-fire runoff simulation.

Table 1
Area and percent area in each burn severity class within the model application area.

Burn severity	Area (km^2)	Percent
Unburned	118.7	42.1
Low Burn	35.3	12.5
Moderate Burn	108.6	38.5
Severe Burn	19.4	6.9

3.2. *Soil permeability data*

Soil data were primarily from the U.S. Department of Agriculture (USDA) SSURGO database, which contains survey information collected by the National Cooperative Soil Survey over the course of the past century at scales ranging from 1:12,000 to 1:63,360. A total of 70 soil units were represented within the project model area. For each soil unit, a range of typical hydraulic conductivities was provided by the SSURGO database. The average of the range of minimum and maximum hydraulic conductivity values for each soil type was assumed to be representative of the hydraulic conductivity for that soil type. Given this assumption, the soil hydraulic conductivity is greater than 9.5 mm/h for more than 95% of the project area, with the majority of the study area having a hydraulic conductivity of 26.2 mm/h or above (Fig. 4). The highest precipitation intensity in this area between 2000 and 2018 was 11.0 mm/h, so saturation-excess overland flow is expected to be the dominant mechanism for initiating overland flow in the project water-shed under pre-fire conditions.

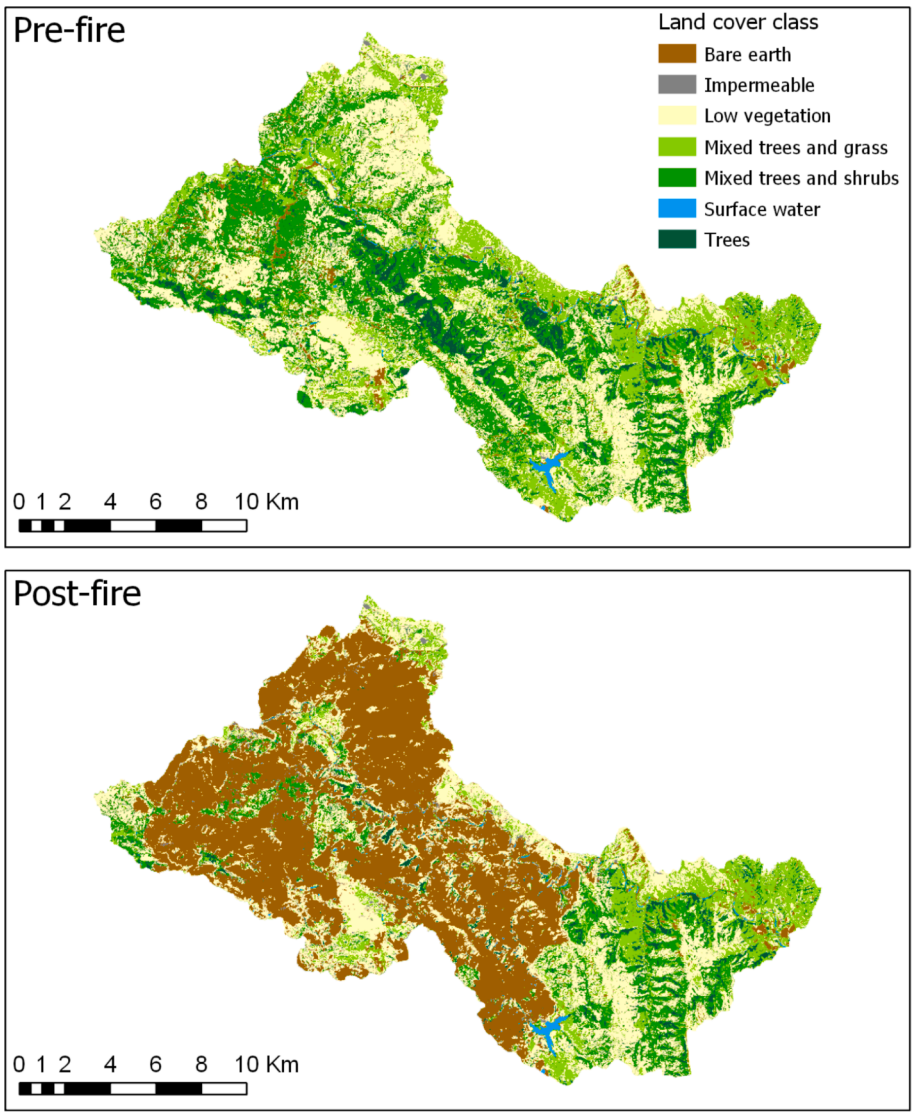

Fig. 3. Pre- and post-fire land cover classifications for the model application area showing the major vegetation categories and the extent of the burn area in 2015.

3.3. Stream flow, climatology and weather data

Hourly Streamflow data at Rumsey for model calibration were downloaded from the U.S. Geological Survey (USGS) National Water Information System (NWIS) (station 11451800) (Fig. 1). California Department of Water Resources (DWR) station RUM was used for discharge data during Water Years 2000, 2015 (http://cdec.water.ca. gov/dynamicapp/staMeta?station_id¼RUM). USGS took over opera-tions of this station as USGS gage 11451800 from September 23rd, 2015.

The UFORE-Hydro and PFHydro models require hourly time series precipitation and potential evapotranspiration (PET) rates for the whole watershed. The models also require time series potential evaporation (PE) rates for trees and short vegetation, leaf area index (LAI) values, and the dates of leaf emergence and leaf fall for each year to quantify vegetation interception of precipitation.

Hourly climate station data are sparse in the area and cannot capture the variability of elevation and local climatology patterns. Hourly climate grids of precipitation and air temperature were developed using eleven local climate stations to represent the spatial heterogeneity of the watershed. An existing FORTRAN-based program was edited to input hourly station data and interpolate the data over the watershed using a geospatial algorithm and a knowledge-based climate product called Parameter-elevation Regressions on Independent Slopes Model (PRISM, http://prism.oregonstate.edu/).

Hourly PET was developed for the study area using hourly air temperature grids and the Priestley-Taylor evapotranspiration equation (Priestley and Taylor, 1972), which considers topographic shading, solar radiation, atmospheric parameters, and cloudiness (Flint et al., 2013). Hourly PE for short vegetation (assumes average height of short vege-tation is 2 m) was calculated using the Priestley-Taylor equation, which assumes a wetted surface (Flint and Childs, 1991). Hourly PE for trees (assumes average height of trees is 10 m) was calculated using the Penman-Monteith equation (Shuttleworth, 1993) and verified using Holmes (2015) equation and local hourly wind data.

Annual LAI values were developed from MODIS (Moderate Resolu-tion Imaging Spectroradiometer; Myneni et al., 2015) remotely sensed data. Leaf-on and leaf-off dates were developed using eMODIS NDVI grids (Swets et al., 1999; Jenkerson et al., 2010; https://phenology.cr. usgs.gov). Hourly gridded climate (precipitation and potential evapo-transpiration), LAI values, and leaf on/off dates were provided as inputs to the UFORE-Hydro and PFHydro model. The meteorological data were averaged over the model domain (Fig. 1) to provide a time series input.

Table 2
Areas and percentages of land use in each burn severity class and vegetation classification for the total modeling area showing a significant reduction in live vegetation post-fire.

Burn Severity	Class Name	Pre-fire		Post-fire	
		Area (km^2)	Percent	Area (km^2)	Percent
Total	Trees	87.4	30.9	37.1	13.2
	Low Vegetation	183.8	65.1	107.7	38.2
	Impermeable	0.6	0.2	2.6	0.9
	Surface water	1.5	0.5	1.6	0.6
	Bare earth	9.2	0.3	132.6	57.1
Unburned	Trees	33.0	27.8	32.9	27.8
	Low Vegetation	78.4	66.1	78.4	66.1
	Impermeable	0.6	0.5	0.6	0.5
	Surface water	1.1	0.9	1.1	0.9
	Bare earth	5.5	4.6	5.5	4.6
Low burn	Trees	10.2	29.0	2.6	7.4
	Low Vegetation	22.8	64.8	18.4	52.3
	Impermeable	0.0	0.1	1.1	3.1
	Surface water	0.3	0.8	0.2	0.7
	Bare earth	1.9	5.3	12.9	36.5
Moderate burn	Trees	33.1	30.5	1.5	1.4
	Low Vegetation	73.5	67.8	10.0	9.3
	Impermeable	0.0	0.0	0.8	0.7
	Surface water	0.1	0.1	0.2	0.2
	Bare earth	1.8	1.7	95.9	88.4
Severe burn	Trees	10.9	56.4	0.1	0.7
	Low Vegetation	8.5	43.6	0.8	4.3
	Impermeable	0.0	0.0	0.1	0.5
	Surface water	0.0	0.0	0.0	0.2
	Bare earth	0.0	0.1	18.3	94.3

3.4. Use of USGS HSPF model to provide the UFORE-Hydro and PFHydro boundary conditions

The Hydrological Simulation Program – FORTRAN (HSPF) rainfall-runoff model (Bicknell, 2001)was used to provide time series of hour-ly flow at the three tributaries upstream of the UFORE-Hydro, PFHydro model domain as boundary conditions (Fig. 1). An HSPF model of the Sacramento River Basin (Stern et al., 2016) was modified to include the model domain shown in Fig. 1, and was calibrated using data from Water Years (WY: October 1-September 30) 2015–17. The HSPF modeling watershed outlet is Rumsey, which is the same station used for calibration of the UFORE-Hydro and PFHydro models, but the HSPF model domain includes a larger contributing area that overlaps the UFORE-Hydro, PFHydro model domain (Fig. 1). The HSPF Nash-Sutcliffe modeling Efficiency (NSE) for hydrograph simulation at Rumsey was 0.87 for WY 2015 – WY 2017 (Stern et al., 2019). The NSE compares the model simulation to observations and tends to emphasize calibration with respect to higher flows (Nash and Sutcliffe, 1970).

4. Results of the models' application

The UFORE-Hydro and PFHydro models were applied to the sub area of the Upper Cache Creek Watershed discussed in the previous section for pre- and post-fire conditions, respectively. The simulation time step is one hour. A Dell laptop with a processor: Intel(R) Core (TM) i7-8850H CPU @ 2.6 GHz, 2.59GHZ, and RAM of 32.0 GB was used for the modeling work. The simulation time for one water year is several sec-onds for the two models.

Three objective functions were used to evaluate model performance for both UFORE-Hydro and PFHydro: The NSE (described above), CRF2 statistic (Equation (14)), and CRF3 statistic (Equation (15)). The CRF2 statistic puts more emphasis on simulation accuracy at every time step (Ye et al., 1997), whereas CRF3 is biased to place more importance on lower flows (Perrin et al., 2001). The value 1.0 of NSE, CRF2, CRF3 means 100% match between simulation and observation. The results of these comparisons are discussed in Sections 4.1 and 4.2.

$$CRF2 = 1 - \sum_{i=1}^{n} \left| Q_{obs,\,i} - Q_{cali} \right| \Big/ \sum_{i=1}^{n} \left| Q_{obs,\,i} - Q_{aveobs} \right| \tag{14}$$

$$CRF3 = 1 - \sum_{i=1}^{n} \left(\sqrt{Q_{obs,i}} - \sqrt{Q_{cal,i}} \right)^2 \Big/ \sum_{i=1}^{n} \left(\sqrt{Q_{obs,i}} - \sqrt{Q_{aveobs}} \right)^2 \tag{15}$$

where $Q_{obs,I}$ is the observed flow at time step i, $Q_{cal,i}$ is the model calculated flow at time step i, Q_{aveobs} is the average observed flow for the whole simulation period, and n is the number of time steps.

4.1. UFORE-hydro pre-fire runoff model calibration and validation

The WY 2000 (10/1/1999–9/30/2000) was selected for calibration

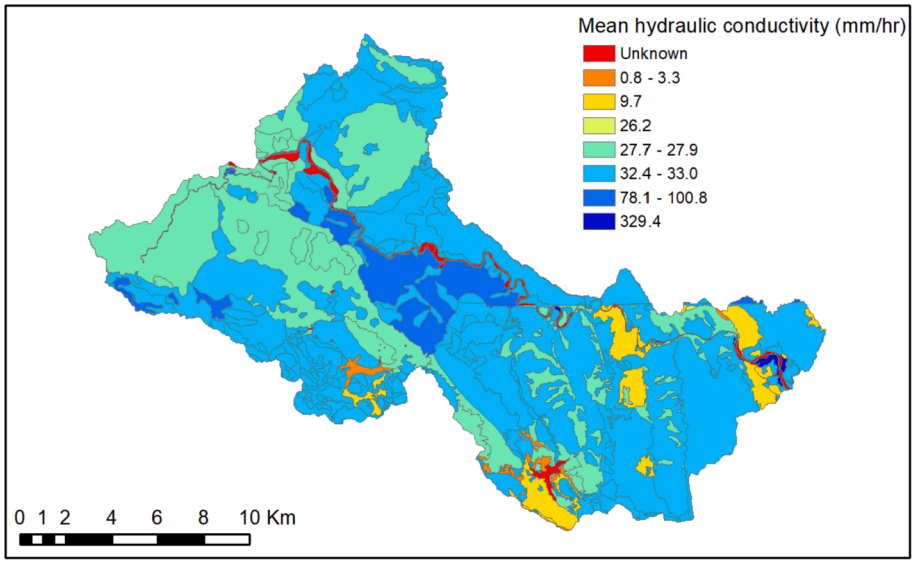

Fig. 4. Hydraulic conductivities for major soil units over the project area.

of the UFORE-Hydro pre-fire model. The NSE, CRF2 and CRF3 were 0.82, 0.64 and 0.88 respectively for the WY 2000 runoff simulation (Fig. 5). The Rocky Fire (07/29/2015–08/14/2015) and Jerusalem Fire (08/09/2015–08/25/2015) occurred near the end of WY 2015. There was no precipitation in WY 2015 that occurred after these fires; therefore, the entire water year could be considered a pre-fire water year. The UFORE-Hydro model was validated to WY 2015 (10/1/2014–09/30/ 2015) using the parameters obtained in the model calibration for WY 2000. The model performance metrics produced the following results: NSE = 0.88, CRF2 = 0.63, CRF3 = 0.80. Fig. 6 shows the hydrograph for WY 2015 and shows storm events at the Rumsey outlet in the Upper Cache Creek Watershed. The parameters used in the calibrated and validated pre-fire hydrological model are listed in Table 3.

4.2. PFHydro model calibration and validation

The PFHydro model was calibrated for WY 2016 (10/1/2015–9/30/2016) (Fig. 7), which was the first water year after the Rocky and Jerusalem fires. The three objective functions for the simulation are as follows: NSE = 0.88, CRF2 = 0.78, CRF3 = 0.91. PFHydro was then validated for WY 2017 (10/1/2016–9/30/2017) (Fig. 8). The three objective functions for the simulation are as follows: NSE = 0.93, CRF2 = 0.81, CRF3 = 0.92. The calibration and validation results indi-cate good model fit to the observations for the pre- and post-fire runoff simulations.

The parameters used in simulations with the calibrated and validated PFHydro model are listed in Table 4.

The PFHydro model assumed that the SWR effects were still present for the WY 2016 and WY 2017. However, the SWR hydrophobic effects were expected to decrease in the 2nd year post-fire (WY, 2017) relative to the 1st year post-fire (WY, 2016). It follows that the hydraulic conductivity of SWR soil should have increased correspondingly in the 2nd year post-fire compared to the soil hydraulic conductivity exhibited in the 1st year. The connectivity of the SWR Patches (Φ) should have also decreased.

The parameters, including the two new parameters (μ and Φ) were tweaked manually for overall best model performance which was evaluated using the three objective functions discussed previously during model calibration and validation. The parameters of the model calibration for WY 2016 and WY 2017, provided in Table 4, support the assumptions made above. For example, the value of μ in the calibrated hydraulic conductivity parameter μK_0 for WY 2017 doubled compared to WY 2016, to 0.2 from 0.1. The connectivity of SWR patches for WY 2017 (Φ = 0.60) was lower than for WY 2016 (Φ = 0.75). The model parameter values for the pre-fire and post-fire models were identical except for these two values that are used to characterize burned soil (μ and Φ) and the values of two parameters for model initial conditions (Initial Stream Discharge and Initial Root Zone Deficit).

5. Discussion

5.1. Pre-fire and post-fire vegetation interception effects

Vegetation interception of precipitation is a function of the vegetation canopy as well as precipitation intensity and duration. As previously discussed, vegetation interception capacity also depends on vegetation interception storage. Once the available vegetation storage is filled, no additional precipitation can be intercepted. Interception typically resumes after the intercepted water has evaporated and interception storage is made available. Interception is a dynamic pro-cess, with vegetation typically intercepting a greater fraction of pre-cipitation for small, scattered storms than for larger, intense storms. The vegetation interception modeling results pre-fire (WY 2000 and WY 2015) and post-fire (WY 2016 and WY 2017) are presented in Table 5.

Water years 2000, 2015, and 2016 had similar annual precipitation totals. For WY 2015 the simulated interception by trees for tree-covered area in the watershed was 82 mm (14.2% of the total precipitation). The high intensity nature of some of the precipitation events and the fact that precipitation during the WY 2015 was concentrated in only two storm events resulted in the lowest interception of the years of precipitation. Annual precipitation during WY 2017 was about 40% higher than the other water years; precipitation intensity was also highest and the per-centage of tree interception simulated by the model was the lowest (about 12% of

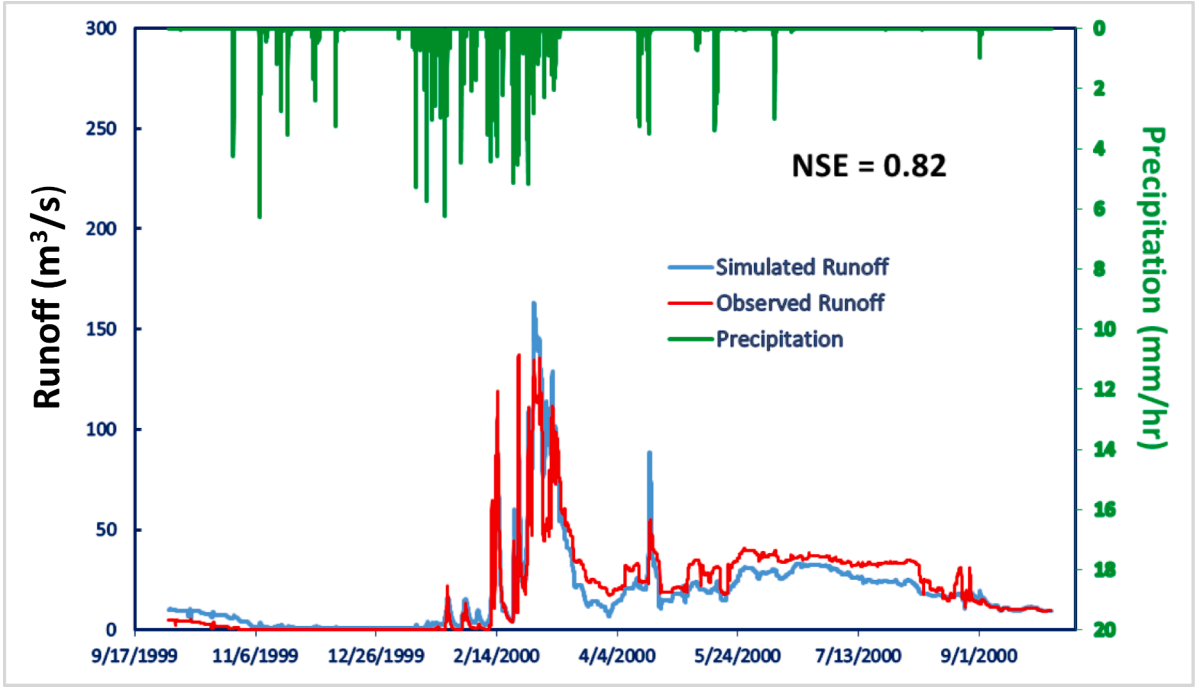

Fig. 5. Hydrograph showing comparison of observed and UFORE-Hydro model simulated pre-fire runoff in the Upper Cache Creek Watershed (Rumsey outlet) for WY 2000.

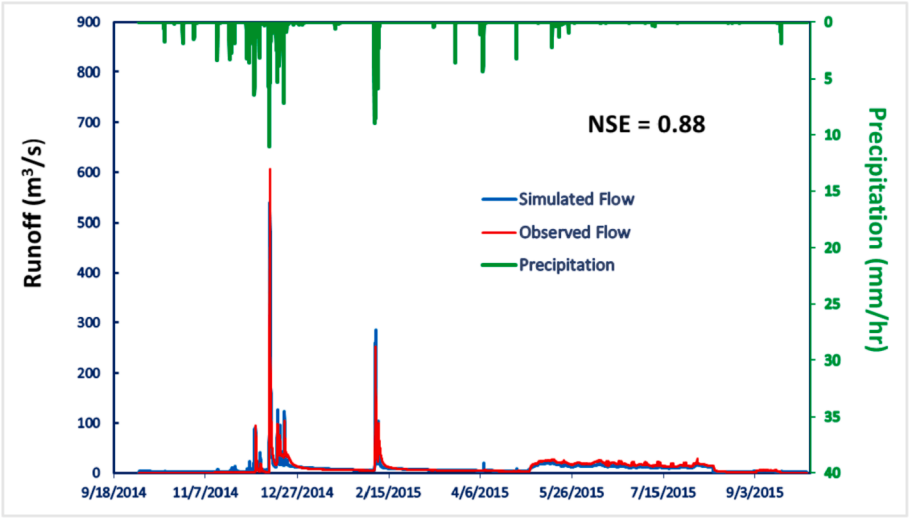

Fig. 6. Hydrograph showing comparison of observed and UFORE-Hydro model simulated pre-fire runoff in the Upper Cache Creek Watershed (Rumsey outlet) for WY 2015.

Table 3
Calibrated and validated pre-fire UFORE-Hydro model parameters in the model study area in the Upper Cache Creek Watershed.

Parameter	Value	Parameter	Value
Scale Parameter of Soil: m (m)	0.0116	Main Channel Routing velocity (m/h)	900
Transmissivity at Saturation: T_0 (m^2/h) Unsaturated Zone	0.39	Internal Channel Routing Velocity (m/h)	950
Delay: T_d (h)	10	Fraction of watershed generating infiltration excess overland flow (decimal %)	0.10
Maximum Root Zone Storage Deficit (m)	0.0064	Saturated surface hydraulic conductivity K_0: (m/h)	0.001
Initial Stream Discharge: (m/h)	3e-06 (WY 2000) 3.5e-06 (WY 2015)	Wetting Front Suction (m)	0.3
Initial Root Zone Deficit (m)	0.006 (WY 2000) 0.006 (WY 2015)	Wetted Moisture Content (decimal %)	0.38

The total precipitation interception of trees for the tree-covered area in WY 2000 (20.2%) and WY 2016 (19.8%) are very similar. However, the total vegetation (trees + short vegetation) interception of rainfall post-fire (4.6%) for the entire model domain in WY 2016 was about 50% of that pre-fire value (9.3%) in WY 2000 because of reduced vegetation in the modeling area due to the fire.

5.2. Post-fire soil water repellent effects on runoff generation

Simulated runoff for the four water years 2000, 2015, 2016 and 2017 is summarized in Table 6. The results displayed in Table 6 show that the percentage of surface runoff in total runoff was highest (49.8%) in WY 2016 (the 1st year post-fire) and 2nd highest (24.5%) in WY 2017 (the 2nd year post-fire). The simulated annual surface runoff was about 6 times greater in WY 2016 than in WY 2000 with similar total precipi-tation for the two WYs. The results support the hypothesis that burning causes SWR-related hydrophobic effects that increase surface runoff, and that SWR decreases with time.

The total runoff during WY 2016 (1st year post-fire, was expected to be higher than the runoff during WY 2015, given that the precipitation in WY 2016 was 630 mm compared with precipitation of 580 mm in WY 2015. However, the total observed and simulated runoff was found to be higher in WY 2015 compared with WY 2016 because the precipitation

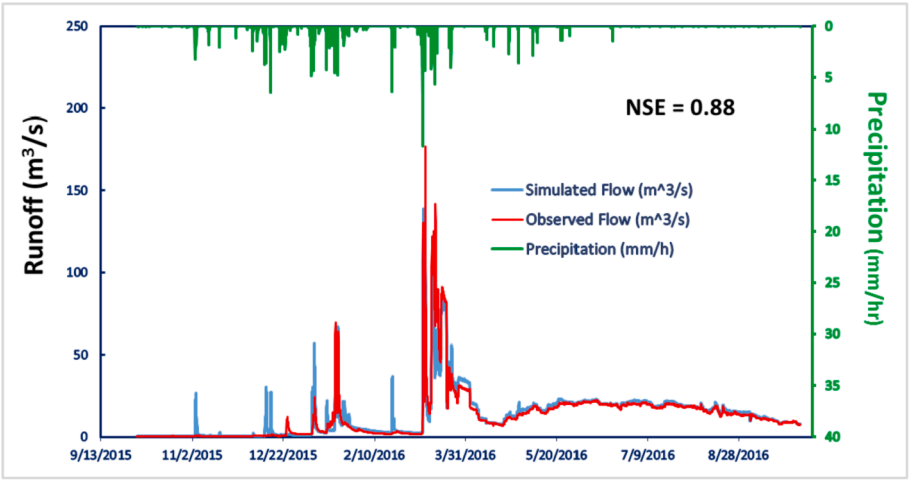

Fig. 7. Hydrograph showing a comparison of observed and PFHydro simulated post-fire runoff at Upper Cache Creek Watershed (Rumsey outlet) for WY 2016.

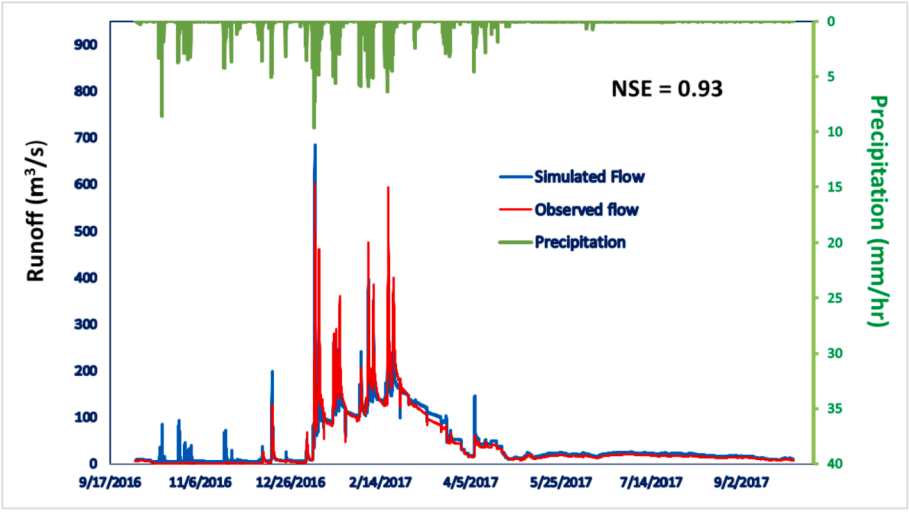

Fig. 8. Hydrograph showing a comparison of observed and PFHydro simulated post-fire runoff at Upper Cache Creek Watershed (Rumsey outlet) for WY 2017.

Table 4
Parameters of the PFHydro post-fire model calibration and validation.

Parameter	Value	Parameter	Value
Scale Parameter of Soil: m (m)	0.0116	Main Channel Routing Velocity (m/h)	900
Transmissivity at Saturation: T_0 (m^2/h) Unsaturated Zone Delay: T_d (h)	0.39 10	Internal Channel Routing Velocity (m/h) Fraction of unburned watershed generating infiltration excess overland flow (decimal %) Saturated surface hydraulic conductivity K_o: (m/h)	950 0.10 0.001
Maximum Root Zone Storage Deficit (m)	0.0064		
Initial Stream Discharge: (m/h)	2e-06 (WY 2016) 5e-06 (WY 2017)	Wetting Front Suction (m)	0.3
Initial Root Zone Deficit (m)	0.0055 (WY 2016) 0.0055 (WY 2017)	Wetted Moisture Content	0.38
High Burn Severity Fraction of K_o: μ *(decimal %)*	0.1 (WY 2016) 0.2 (WY 2017)	Connectivity of SWR Patches: Φ *(decimal %)*	0.75 (WY 2016) 0.60 (WY 2017)

during WY 2015 was concentrated in fewer major storm events than during WY 2016. The simulated surface runoff, on the other hand, was about 1.6 times greater in WY 2016 than in WY 2015, emphasizing the importance of post-fire SWR hydrophobic effects.

Surface runoff simulated by PFHydro for the burned areas is shown in Table 7 (far right column). The normalized precipitation and runoff totals were compared. During WY 2016, the simulated surface runoff of 120 mm over the burned area comprised 47% of the total runoff (257 mm) and 93% of the surface runoff (128 mm). The simulated surface runoff for WY 2017 from the burned area was 186 mm, which was about 17% of total runoff (962 mm) and 79% of the total surface runoff (236 mm). Therefore, the SWR hydrophobic effects on precipitation-induced runoff diminished during the 2nd year post-fire compared to the 1st year post-fire.

Given the variation in precipitation volume, intensity, and duration between WY 2016 and WY 2017, it is difficult to draw overarching conclusions from two years of watershed runoff data and the comparison of pre-fire and post-fire conditions as they relate to the total annual runoff.

Two large storm events, one pre-fire (in WY 2015) and one post-fire (in WY 2017), were identified as having the same duration and similar precipitation amounts and intensities. A comparison of model predictions and field observations for the two storm events is shown in Fig. 9 and Table 8, which helps validate the previously described conceptual model of post-fire runoff generation.

The two storms analyzed were the first large storms during the wet seasons of WY 2015 and WY 2017 and the two storms had the same precipitation duration (58 h). The total precipitation for the pre-fire storm (124 mm) and the maximum rainfall intensity (10.9 mm/h)

Table 5
Results of model simulations of vegetation interception (of precipitation) for pre-fire and post-fire.

Water Year	Annual Precipitation (mm)	Annual Interception of Trees for Tree-Covered Area (mm)	Annual Interception of Trees for Entire Model Domain	Annual Interception of Short Vegetation for Entire Model Domain	Annual Interception of All Vegetation for Entire Model Domain
2000 (pre-fire)	672	136 (20.2%)	6.3%	3%	9.3%
2015 (pre-fire)	580	82 (14.2%)	4.4%	2.3%	6.7%
2016 (post-fire)	630	125 (19.8%)	2.8%	1.8%	4.6%
2017 (post-fire)	1118	134 (12%)	1.7%	1.1%	2.8%

Table 6
Simulated surface, subsurface and total runoff of WYs 2000, 2015, 2016, and 2017 for the modeling area in the Upper Cache Creek Watershed.

Water Year	Annual Precipitation (mm)	Total Simulated Flow (m^3/s)	Total Simulated Surface Flow (m^3/s)	Total Simulated Subsurface Flow (m^3/s)	Percentage of Surface flow in Total flow
2000 (pre-fire)	672	21445	1852	19419	8.6%
2015 (pre-fire)	580	41071	6264	34619	15.2%
2016 (post-fire)	630	20142	10026	10110	49.8%
2017 (post-fire)	1118	75447	18491	56944	24.5%

Table 7
Comparison of surface and subsurface runoff from burned areas during WYs 2016, 2017.

Water Year	Total Precipitation (mm)	Total Surface and Subsurface Runoff (mm)	Total Subsurface Runoff (mm)	Total Surface Runoff (mm)	Total Surface Runoff from Burned Area (mm)
2016	630	257	129	128	120
2017	1118	962	726	236	186

were higher than for the post-fire storm (122 mm and 9.6 mm/h, respectively). However, the total post-fire storm event runoff was about 1.7 times that of the total pre-fire storm event.

The modeled storm runoff quantities were very close to the observations for both storms (Table 10). Likewise, the modeled pre-fire and post-fire storm runoff volumes, when compared with observations, were only 0.39% higher and 0.21% lower, respectively. The shape of the model-simulated hydrographs for the two storms also show a good match to observations (Fig. 9). Although surface runoff from the watershed cannot be directly measured, the excellent match between the quantity and timing of observations and model simulated total runoff suggest a valid conceptual and numerical model. The total surface runoff simulated with the post-fire model simulation was about 1.8 times greater than the surface runoff simulated with the pre-fire model.

The good match between field observations and model simulated runoff values suggests that the post-fire SWR soil hydrophobic effects still existed at the time of this storm, which was about 17 months after the fires occurred. This result supports the model assumption that the soil SWR layer was still present during WY 2017.

5.3. Sensitivity analyses of μ and Φ

Sensitivity analyses of parameters μ and Φ simulating SWR effects are presented in Tables 9 and 10, respectively.

It can be seen from Table 9 that the surface flow decreases, and subsurface flow increases with increased μ (fraction of K_{sat} in unburned area) because of a higher infiltration. The annual total flow also de-creases with increased μ but at a much smaller scale.

The two most sensitive changes of μ are from 0.3 to 0.4 and from 0.6 to 0.7, causing surface runoff decreases of 26.0%, 29.4%, respectively.

It can be seen from Table 10 that the surface flow increases almost constantly (from 15.5 to 15.8 mm) with the increase of Φ (connectivity of burned patches), whereas the percent increase decreases. The SWR effect is minimal or can be neglected when Φ is zero. Note that there is about 42% unburned area which has no SWR effect in the modeling

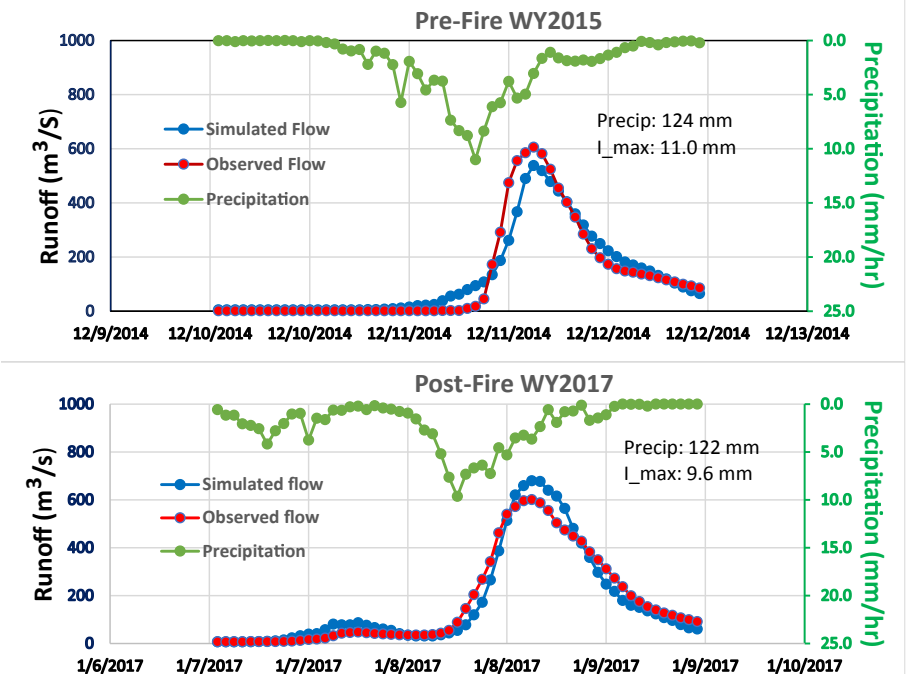

Fig. 9. Comparison of model runoff simulations for similar pre-fire and post-fire storm events. "Precip" is total storm event precipitation, "I_max" is the maximum precipitation intensity.

Table 8
Comparison of model results for the pre-fire and post-fire storm events.

Precipitation Start, End (Duration = 58 h)	Total precipitation (mm)	Total observed runoff (m^3/s)	Total simulated runoff (m^3/s)	Total simulated surface runoff (m^3/s)	Surface runoff/total runoff
12/10/14 1:00 a.m.–12/12/14 11:00 a.m. (Pre-fire)	123.7	2363	2372	1948	82.1%
01/07/17 1:00 a.m. – 01/09/17 11:00 a.m. (Post-fire)	122.0	3955	3947	3493	88.5%

Table 9
Sensitivity analysis of parameter μ on runoff generation for WY 2016. Δ Surface Flow is the change in surface flow relative to the previous smaller value of μ.

μ	Annual Surface Flow (mm)	Annual Subsurface Flow (mm)	Annual Total Flow (mm)	Δ Surface Flow (mm)	Δ Surface Flow (%)
0.1	127.8	128.9	256.7	–	–
0.2	116.3	134.9	251.2	−11.5	−9.0
0.3	99.8	144.6	244.4	−16.5	−14.2
0.4	73.9	162.4	236.3	−25.9	−26.0
0.5	64.1	169.1	233.3	−9.8	−13.3
0.6	58.8	172.8	231.6	−5.3	−8.3
0.7	41.5	185.1	226.6	−17.3	−29.4

Table 10
Sensitivity analysis of parameter Φ on runoff generation for WY 2016. Δ Surface Flow is the change in surface flow relative to the previous smaller value of Φ.

Φ	Annual Surface Flow (mm)	Annual Subsurface Flow (mm)	Annual Total Flow (mm)	Δ Surface Flow (mm)	Δ Surface Flow (%)
0.0	10.6	207.2	217.8	–	–
0.1	26.2	195.6	221.8	15.6	147.2
0.2	41.7	184.7	226.4	15.5	59.2
0.3	57.3	174.0	231.3	15.6	37.4
0.4	72.8	163.6	236.4	15.5	27.1
0.5	88.5	153.3	241.8	15.7	21.6
0.6	104.2	143.3	247.5	15.7	17.7
0.7	119.9	133.6	253.5	15.7	15.1
0.8	135.6	124.4	260.0	15.7	13.1
0.9	151.4	115.4	266.9	15.8	11.7
1.0	167.2	107.0	274.2	15.8	10.4

domain.

6. Summary and conclusions

The results of this study suggest that the UFORE-Hydro and PFHydro models were properly calibrated and validated for simulations of pre- fire and post-fire runoff (Table 11). The model performance statistics considered (NSE, CRF2, and CRF3) confirm the agreement between the models and field observations.

Model simulations show that precipitation interception by vegetation was reduced by wildfires, as expected (Table 5). When water years with similar annual precipitation volumes and rainfall characteristics were compared, post-fire vegetation interception in WY 2016 was about 50% lower than pre-fire vegetation interception in a comparable year like WY 2000. Fire-induced SWR hydrophobic effects on precipitation- induced runoff generation have been demonstrated using the results of annual model simulations which produced greater surface runoff and a reduction in subsurface flow (Table 6) when pre-fire and post-fire con-ditions were compared. Two storm events during the modeled period that showed high similarity were selected to compare pre-fire and post- fire conditions, which clearly demonstrated the post-fire SWR effects. The simulation results showed that both surface runoff and total runoff significantly increased post-fire (Table 8).

The UFORE-Hydro model was enhanced to create PFHydro with a new model structure and new algorithms simulating burn effects from wildfire that resulted in a good match between modeling results and measured field observations for post-fire conditions. The PFHydro model provides a unique and reliable way to simulate post-fire watershed scale hydrological process and precipitation-induced runoff.

Table 11
Model runoff simulation calibration and validation results.

Water Year	NSE	CRF2	CRF3	
2000	0.82	0.64	0.88	Pre-fire calibration
2015	0.88	0.63	0.80	Pre-fire validation
2016	0.88	0.78	0.91	Post-fire calibration
2017	0.93	0.81	0.92	Post-fire validation

7. Further work

The current model was applied to the Upper Cache Creek Watershed, which was assumed to be homogenous. The model will be updated so that it can be applied it to a heterogeneous watershed. In the natural environment soil water repellency (SWR) significantly decreases with increasing soil moisture. For simplicity, the current model assumes SWR remains for the first two years post-fire and remains constant within a single year. An algorithm will be developed to simulate the soil moisture content dynamically year-round to simulate post-fire SWR effects more accurately.

Because large fires affected the Upper Cache Creek Watershed during summer 2018, there will be opportunities to use results of planned monitoring during Water Years 2019, 2020 to further test the PFHydro model. Ongoing work also includes using the HSPF and PFHydro models to simulate the transport of suspended sediment and mercury, a signif-icant contaminant in the Upper Cache Creek Watershed.

Declaration of competing interest

This message is regard to the manuscript “PFHydro: A New Watershed-Scale Model for Post-Fire Runoff Simulation” (Ref: ENVSOFT_2019_562) submitted to Environmental Modeling and Software.

All authors declare that there is no conflicts of interest.

Acknowledgements

The researchers gratefully acknowledge funding support from the U. S. Bureau of Reclamation through the Science and Technology Program and U.S. Bureau of Land Management. This work is part of the research project: Research and Development of a Watershed-Scale Model/Tool for Simulating the Effects of Wildfires on Mercury Contamination of Land and Water.

References

Agnew, W., Labn, R.E., Harding, M.V., 1997. Buffalo Creek, Colorado, fire and flood of 1996. Land Water 41, 27–29.

Ambroise, B., Beven, K., Freer, J., 1996. Toward a generalization of the TOPMODEL concepts: topographic indices of hydrological similarity. Water Resour. Res. 32 (7), 2135–2145.

Benavides-Solorio, J.D.D., MacDonald, L.H., 2005. Measurement and prediction of post-fire erosion at the hillslope scale, Colorado Front Range. Int. J. Wildland Fire 14, 457–474. https://doi.org/10.1071/WF05042.

Beven, K.J., Kirkby, M.J., 1979. A Physically based variable contributing area model of basin hydrology. Hydrol. Sci. Bull. 24 (1), 43–69.

Beven, K.J., 1984. Infiltration into a class of vertically non-uniform soils. Hydrology Science Journal 29, 425–434.

Beven, K. (Ed.), 1997. Distributed Hydrological Modeling: Applications of the Topmodel Concept Advances in Hydrological Processes. Wiley, West Sussex, Engla.

Beven, K.J., 1997. TOPMODEL: a critique. Hydrol. Process. 11, 1069–1085. Bicknell, B.R., Imhoff, J.C., Kittle Jr., J.L., Jobes, T.H., Donigian Jr.,A.S.,, 2001.

Hydrological Simulation Program - Fortran (HSPF), User's Manual for Release 12. U. S. EPA National Exposure Research Laboratory, Athens, GA, in cooperation with U.S. Geological Survey, Water Resources Division, Reston, VA.

Blake, W.H., Theocharopoulos, S.P., Skoulikidis, N., Clark, P., Tountas, P., Hartley, R., Amaxidis, Y., 2009. Wildfire impacts on hillslope sediment and phosphorus yields. J. Soils Sediments 10, 671–682.

Bond, R.D., 1964. The influence of the microflora on the physical properties of soils. II. Field studies on water repellent sands. Aust. J. Soil Res. 2, 111–122.

Cawson, J., Sheridan, G., Lane, P., Smith, H., 2010. Characterising fire severity patches to understand how burn patchiness affects runoff connectivity and erosion. Geophys. Res. Abstr. 12. EGU2010-3009.

Cerrelli, G.A., 2005. FIRE HYDRO, a simplified method for predicting peak discharges to assist in the design of flood protection measures for western wildfires. In: GE, Moglen (Ed.), 'Proceedings of the 2005 Watershed Management Conference – Managing Watersheds for Human and Natural Impacts: Engineering, Ecological, and Economic Challenges', July 2005, Williamsburg, VA. American Society of Civil Engineers, Alexandria, VA), pp. 935–941.

Chen, L., Berli, M., Chief, K., 2013. Examining modeling approaches for the rainfall-runoff process in wildfire-affected watersheds: using San Dimas Experimental Forest. J. Am. Water Resour. Assoc. 1–16. https://doi.org/10.1111/jawr.12043.

de Jonge, L.W., Jacobsen, O.H., Moldrup, P., 1999. Soil water repellency: effects of water content, temperature, and particlesize. Soil Sci. Soc. Am. J. 63, 437–442.

DeBano, L.F., 1966. Formation of Non-wettable Soils: Involves Heat Transfer Mechanism, vol. 132. Pacific Southwest Forest & Range Experiment Station.

DeBano, L.F., 1981. Water Repellent Soils: a State of the Art, Gen. Tech. Rpt. PSW-46. USDA For. Serv., Pacific Southwest Forest and Range Exp. Sta., Berkeley, CA, p. 21pp.

Tech. Rpt. PSW-43. USDA For. Serv DeBano, L.F., Osborn, J.F., Krammes, J.S., Letey Jr., J., 1967. Soil Wettability and Wetting Agents…our Current Knowledge of the Problem. Gen. Pacific Southwest Forest and Range Exp. Sta., Berkeley, CA, 13pp.

DeBano, L.F., Krammes, J.S., 1966. Water repellent soils and their relation to wildfire temperatures. International Association of Scientific Hydrology Bulletin 11, 14–19.

DeBano, L.F., Neary, D.G., Ffolliott, P.F., 1998. Fire's Effects on Ecosystems. John Wiley & Sons, Inc., New York, ISBN 978-0-471-16356-5, 333 pp.

Dekker, L.W., Ritsema, C.J., 1995. Fingerlike wetting patterns in two water-repellent loam soils. J. Environ. Qual. 24, 324–333.

Dekker, L.W., Doerr, S.H., Oostindie, K., Ziogas, A.K., Ritthesema, C.J., 2001. Water repellency and critical water content in a dune sand. Soil Sci. Soc. Am. J. 65, 1667–1674.

Doerr, S.H., Moody, J.A., 2004. Hydrological effects of soil water repellency: on spatial and temporal uncertainties. Hydrol. Process. 18, 829–832.

Doerr, S.H., Thomas, A.D., 2000. The role of soil moisture in ity classes. Time since burning was a significant control controlling water repellency: new evidence from forest soils in on the strength of soil water repellency at the soil surface. Portugal. J. Hydrol. (Amsterdam) 231 (–232), 134–147.

Dolan, Jack, January 21, 2018. Search Teams Find 21st Victim of Montecito Mudslide". Los Angeles Times. Retrieved. (Accessed 21 January 2018).

Dunne, T., 1978. Field studies of hillslope flow processes. In: Kirkby, M.J. (Ed.), Hillslope Hydrology. John Wiley & Sons, New York, pp. 227–293.

Ebel, B.A., Moody, J.A., 2012. Rethinking infiltration in wildfire-affected soils. Hydrological Processes. https://doi.org/10.1012/hyp.9696.

Jul 9-12, Portland, OR. Paper No. 068011 Elliot, W.J., Miller, I.S., Glaza, B.D., 2006. Using WEPP technology to predict erosion and runoff following wildfire. In: Presented at the ASAE Annual International Meeting. ASAE, St. Joseph, MI, 12pp.

Elliot, W.J., Hall, D.E., Robichaud, P.R., 2010. FS Peak Flow Calculator. Version 2010.10.28. U.S. Department of Agriculture, Forest Service, Rocky Mountain Research Station, Moscow, ID (online at. http://forest.moscowfsl.wsu.edu/fswepp /ermit/peakflow. last accessed 30 January 2012.

NSERL Report No. 10 Flanagan, D.C., Nearing, M.A., 1995. USDA-water Erosion Prediction Project: Hillslope Profile and Watershed Model Documentation. USDA-ARS National Soil Erosion Research Laboratory, West Lafayette.

Flint, A.L., Childs, S.W., 1991. Use of the Priestley-Taylor evaporation equation for soil water limited conditions in a small forest clear cut. Agric. For. Meteorol. 56 (3–4), 247–260.

Flint, L.E., Flint, A.L., Thorne, J.H., Boynton, R., 2013. Fine-scale hydrological modeling for climate change applications; using watershed calibrations to assess model performance for landscape projections. Ecological Processes 2, 25.

Foltz, Meg, 2008. A WATBAL Watershed Program Input Data and Summary Report for. U.S. Department of Agriculture, Forest Service, Clear water National Forest (Unpublished data supplied to author by M. Foltz, a Clearwater National Forest hydrologist).

Foltz, R.B., Robichaud, P.R., Rhee, H., 2009. A Synthesis of Post-fire Road Treatments for BAER Teams: Methods, Treatment Effectiveness, and Decision Making Tools for Rehabilitation. US Department of Agriculture, Forest Service, Fort Collins, CO). Rocky Mountain Research Station. General Technical Report RMRS-GTR-228.

Frankenberger, J.R., Dun, S., Flanagan, D.C., Wu, J.Q., Elliot, W.J., 2011. Development of a GIS interface for WEPP model application to Great Lakes forested watersheds. In: Proc. Intl. Symp. On Erosion and Landscape Evolution. ASABE, St. Joseph, Mich, p. 11139.

Garbrecht, J., Martz, L.W., 1997. TOPAZ Version 1.20: an Automated Digital Landscape Analysis Tool for Topographic Evaluation, Drainage Identification, Watershed Segmentation and Subcatchment Parameterization - Overview. Rep.# GRL, vols. 97–2. Grazinglands Research Laboratory, USDA, Agricultural Research Service, El Reno, Oklahoma, 21 pp.

July 19-22 Goodrich, D.C., Canfield, H.E., Burns, I.S., Semmens, D.J., Hernandez, M., Levick, L.R., Guertin, D.P., Kepner, W., 2005. Rapid post-fire hydrologic watershed asessment using the AGWA GIS-based hydrologic modeling tool. In: Proc. ASCE Watershed Manage. Conf. CD-ROM, Williamsburg, VA, 12pp.

Hamilton, E.L., Rowe, P.B., 1949. Rainfall Interception by Chaparral in California. USDA and California Dep. Natur. Resour. Div. Forestry (Unnumbered Pub).

Hawkins, R.H., Greenberg, R.J., 1990. WILDCAT4 Flow Model. University of Arizona, School of Renewable Natural Resources, Tucson, AZ.

Hawkins, R.H., Munoz, A.B., 2011. Wildcat 5 for Windows (W5W): Documentation and Manual. University of Arizona, School of Natural Resources and Environment, Tucson, AZ.

Holmes, J.D., 2015. Wind Loading of Structures, third ed. CRC Press, Boca Raton, FL. 413 pp.

Holzhey, C.S., 1969. Water-repellent soil in southern California. In: DeBano, L.F., Letey, J. (Eds.), Water-Repellent Soils: Proceedings, Riverside, CA, pp. 31–41. Huffman, E.L., MacDonald, L.H., Stednick, J.D., 2001. Strength and persistence of fire-induced soil hydrophobicity under pon-derosa and lodgepole pine, Colorado Front Range. Hydrol. Process. 15, 2877–2892.

Imeson, A.C., Verstraten, J.M., vanMulligan, E.J., Sevink, J., 1992. The effects of fires and water repellency on infiltration and runoff documented previously, but is consistent with our un- under Mediterranean type forest. Catena 19, 345–361. Inbar, M., Tamir, M., Wittenberg, L., 1998. Runoff and erosion processes after a forest fire in Mount Carmel, a Mediterranean area. Geomorphology 24, 17–33. https://doi. org/10.1016/S0169-555X(97)00098-6.

Iorgulescu, I., Musy, A., 1998. Generalization of TOPMODEL for a power law transmissivity profile. Hydrol. Process. 11, 1353–1355.

Jarrett, R.D., England, J.F., House, 2002. Reliability of paleostage indicators for paleoflood studies. In: House, P.K., Webb, R.H., Baker, V.R., Levish, D.R. (Eds.), Ancient Floods, Modern Hazards, Principles and Applications of Paleoflood Hydrology, vol. 5. American Geophysical Union, Water and Science Application, Washington, D.C., pp. 99–110

Jenkerson, C.B., Maiersperger, T.K., Schmidt, G.L., 2010. eMODIS - a User-Friendly Data Source. U.S. Geological Survey (USGS) Open-File Report, Reston, VA, USA, 2010-1055.

Johansen, M.P., Hakonson, T.E., Breshears, D.D., 2001. Post-fire runoff and erosion fromrainfall simulation: contrasting forests with shrub lands and grasslands. Hydrol. Process. 15, 2953–2965.

Kean, J.W., Staley, D.M., Cannon, S.H., 2011. In situ measurements of post-fire debris flows in southern California: comparisons of the timing and magnitude of 24 debris-flow events with rainfall and soil moisture conditions. J. Geophys. Res. 116 https://doi.org/10.1029/2011JF002005 (F04019).

Keizer, J.J., Coelho, C.O.A., Shakesby, R.A., Domingues, C.S.P., Malvar, M.C., Perez, I.M. P., Matias, M.J.S., Ferreira, A.J.D., 2005. The role of soil water repellency in overland flow generation in pine and eucalypt forest stands in coastal Portugal. Aust. J. Soil Res. 43, 337–349.

Kinoshita, A.M., Hogue, T.S., Napper, C., 2014. Evaluating pre-and post-fire peak discharge predictions across western US watersheds. JAWRA Journal of the American Water Resources Association 50 (6), 1540–1557.

Kirkby, M.J., 1997. TOPMODEL: a personal view. Hydrol. Process. 11, 1087–1097.

LACDPW (Los Angeles County Department of Public Works), 1991. Modeling single storm events in small urban areas. https://www.aquaveo.com/software/w ms-modrat.

Letey, J., 2001. Causes and consequences of fire-induced soil water repellency. Hydrol. Process. 15, 2867–2875.

Luce, C.H., 2001. FERGI: fire enhanced runoff and gully initiation model. Available: http://fergi.boise.rmrs.fs.fed.us/fergi/, 2 January 2008.

MacDonald, L.H., Huffman, E.L., 2004. Post-fire soil water repellency: persistence and soil moisture threshold. Soil Sci. Soc. Am. J. 68, 1729–1734.

Martinez-Mena, M., Alvarez, Rogel J., Albaladejo, J., Castillo, V.M., 2000. Influence of vegetal cover on sediment particle size distribution in natural rainfall conditions in a semiarid environment. Catena 38, 175–190. https://doi.org/10.1016/S0341-8162(99)00073-9.

Meeuwig, R.O., 1971. Infiltration and Water Repellency in Granitic Soils. Res. Paper INT-111. USDA For. Serv., Intermountain Res. Sta., Ogden, UT, 10pp.

Miller, M.E., Billmire, M., Elliot, W.J., Endsley, K.A., Robichaud, P.R., 2015. Rapid response tools and datasets for post-fire modeling: linking Earth Observations and process-based hydrological models to support post-fire remediation. Int. Arch. Photogramm. Remote Sens. Spatial Inf. Sci., XL-7/W3 469–476. https://doi.org/10.5194/isprsarchives-XL-7-W3-469-2015.

Miller, M.E., Elliot, W.J., Billmire, M., Robichaud, P.R., Endsley, K.A., 2016. Rapid response tools and datasets for post-fire remediation: linking remote sensing and process-based hydrologic models. Int. J. Wildland Fire (25), 1061–1073.

Report 2011–5236 Moody, J.A., 2012. An analytical method for predicting post wildfire peak discharges. U.S. Geological Survey Scientific Investigations, 36 pp.

Moody, J.A., Martin, D.A., 2001. Post-fire, rainfall intensity-peak discharge relations for three mountainous watersheds in the western USA. Hydrol. Process. 15, 2981–2993. https://doi.org/10.1002/HYP.386.

Moody, J.A., Martin, D.A., 2009. Synthesis of sediment yields after wildland fire in different rainfall regimes in the western United States. Int. J. Wildland Fire 18, 96–115.

Moody, J.A., Martin, D.A., Haire, S.L., Kinner, D.A., 2008. Linking runoff response to burn severity after a wildfire. Hydrol. Process. 22, 2063–2074.

Moody, J.A., Shakesby, R.A., Robichaud, P.R., Cannon, S.H., Martin, D.A., 2013. Current research issues related to post-wildfire runoff and erosion processes. Earth Sci. Rev. 122, 10–37. https://doi.org/10.1016/j.earscirev.2013.03.004.

Morris, S.E., Moses, T.A., 1987. Forest fire and the natural soil erosion regime in the Colorado Front Range. Ann. Assoc. Am. Geogr. 77, 245–254.

Myneni, R., Knyazikhin, Y., Park, T., 2015. MCD15A2H MODIS/Terra+Aqua leaf area index/FPAR 8-day L4 global 500m SIN grid V006. Distributed by NASA EOSDIS land processes DAAC. https://doi.org/10.5067/MODIS/MCD15A2H.006.

Nash, J.E., Sutcliffe, J.V., 1970. River flow forecasting through conceptual models Part I—a discussion of principles. J. Hydrol. 27 (3), 282–290.

Neary, D.G., 2011. Impacts of wildfire severity on hydraulic conductivity in forest, woodland and grassland soils. In: Elange, L. (Ed.), Hydraulic Conductivity—Issues, Determination, and Application. InTech Publishers, Rijeka, Croatia, pp. 123–142.

Neary, D.G., Gottfried, G.J., Folliott, P.F., 2003. Post-wildfire watershed flood responses. In: Proceedings of the 2nd International Fire Ecology Conference, Orlando, FL, pp. 16–20.

Revised 2008 Wildland fire in ecosystems: fire effects on soil and water. In: Neary, D.G., Ryan, K.C., DeBano, L.F. (Eds.), 2005. General Technical Report RMRS-GTR-42, vol. 4. U.S. Department of Agriculture, Forest Service, Rocky Mountain Research Station, Fort Collins, CO, 250 pp.

Nyman, P., Sheridan, G., Lane, P.N.J., 2010. Synergistic effects of water repellency and macropore flow on the hydraulic conductivity of a burned forest soil, south-east Australia. Hydrol. Process. 24, 2871–2887.

Onda, Y., Dietrich, W.E., Booker, F., 2008. Evolution of overland flow after a severe forest fire. Point Reyes, California. Catena 72, 13–20.

Owens, M.K., Lyons, R.K., Alejandro, C.L., 2006. Rainfall partitioning within semiarid juniper communities: effects of event size and canopy cover. Hydrol. Process. 20, 3179–3189. https://doi.org/10.1002/HYP.6326.

Perrin, C., Michel, C., Andréassian, V., 2001. Does a large number of parameters enhance model performance? Comparative assessment of common catchment model structures on 429 catchments. J. Hydrol. 242, 275–301.

Ponce, V.M., 1989. Engineering Hydrology–Principles and Practices. Prentice-Hall, Inc., Englewood Cliffs, New Jersey, p. 642.

Priestley, C.H.B., Taylor, R.J., 1972. On the Assessment of Surface Heat Flux and Evaporation Using Large-Scale Parameters. Monthly Weather Review 100 (2), 81–92. https://doi.org/10.1175/1520-0493(1972)100<0081:OTAOSH>2.3.CO;2.

Renschler, C.S., 2003. Designing geo-spatial interfaces to scale process models: the GeoWEPP approach. Hydrol. Process. 17, 1005e1017.

Ritsema, C.J., Dekker, L.W. (Eds.), 2003. Soil Water Repellency: Occurrence, Consequences, and Amelioration. ISBN-13: 978-0444512697. 358 pp.

Robichaud, P.R., 2000. Fire effects on infiltration rates after prescribed fire in northern Rocky Mountain forests, USA. J. Hydrol. 220–229.

Robichaud, P.R., Lewis, S.A., Ashmun, L.E., 2008. New Procedure for Sampling Infiltration to Assess Post-fire Soil Water Repellency. US Department of Agriculture, Forest Service, Rocky Mountain Research Station. Research Note RMRS-RN-33. (Fort Collins, CO). Available at: http://forest.moscowfsl.wsu.edu/BAERTOOLS/MDI/. Verified 14 April 2012.

Robichaud, P.R., Ashmun, L.E., Foltz, R.B., Showers, C.G., Groenier, J.S., Kesler, J., DeLeo, C., Moore, M., 2013. Production and Aerial Application of Wood Shreds as a Post-fire Hillslope Erosion Mitigation Treatment. Gen. Tech. Rep. RMRS-GTR-307. U. S. Department of Agriculture, Forest Service, Rocky Mountain Research Station, Fort Collins, CO, 31 pp.

Robichaud, P.R., Lewis, S.A., Wagenbrenner, J.W., Ashmun, L.E., Brown, R.E., 2013. Post-fire mulching for runoff and erosion mitigation: Part I: effectiveness at reducing hillslope erosion rates. Catena 105, 75–92.

Rowe, P.B., 1948. Influence of woodland chaparral on water and soil in central California.[N.p.]: state of California Department of Natural Resources. Division of Forestry, incooperation with the U.S. Department of Agriculture, Forest Service, California Forest and Range Experiment Station, 70 pp.

Rowe, P.B., Countryman, C.M., Storey, H.C., 1949. Probable Peak Discharge and Erosion Rates from Southern California Watersheds as Influenced by Fire. Department of Agriculture, Forest Service, PacificSouthwest Forest and Range Experiment Station, Berkeley, California.

Rutter, A.J., Morton, A.J., Robins, P.C., 1971. A predictive model of rainfall interception in forests. I. A derivative of the model from observations in a plantation of Corsican pine. Agric. Meteorol. 9, 367.

Rutter, A.J., Morton, A.J., Robins, P.C., 1975. A predictive model of rainfall interception in forests. II. Generalization of the model and comparison with observations in some coniferous and hard-wood stands. J. Appl. Ecol. 12, 367.

Sacramento River Watershed Program, 2018. Cache Creek watershed. Available online at: http://www.sacriver.org/aboutwatershed/roadmap/watersheds/westside/cache-creek-watershed. Accessed 8/22/2018.

Schmidt, K.M., Hanshaw, M.N., Howle, J.F., Kean, J.W., Staley, D.M., Stock, J.D., Bawden, G.W., 2011. Hydrologic conditions and terrestrial laser scanning of post-fire debris flows in the San Gabriel Mountains, CA. U.S.A Italian Journal of Engineering Geology and Environment. https://doi.org/10.4408/IJEGE.2011-03.B-064.

Shakesby, R.A., Doerr, S.H., Walsh, R.P.D., 2000. The erosional impact of soil hydrophobicity: current problems and future research directions. J. Hydrol. 231–232, 178–191.

Shuttleworth, W.J., 1993. Evaporation. In: Maidment, D.R. (Ed.), Handbook of Hydrology. McGraw-Hill, Inc, 1993.

Skau, C.M., 1964. Interception, throughfall, and stemflow in Utah and alligator juniper cover types in northern Arizona. For. Sci. 10, 283–287.

Smith, H.G., Sheridan, G.J., Lane, P.N., Nyman, P., Haydon, S., 2011. Wildfire effects on water quality in forest catchments: a review with implications for water supply. J. Hydrol. 396 (1–2), 170–192. https://doi.org/10.1016/J.JHYDROL.2010.10.043.

Spigel, K.M., Robichaud, P.R., 2007. First-year post-fire erosion rates in the Bitterroot National Forest, Montana. Hydrol. Process. 21, 998–1005. https://doi.org/10.1002/HYP.6295.

Stern, M., Flint, L., Minear, J., Flint, A., Wright, S., 2016. Characterizing changes in streamflow and sediment supply in the Sacramento River basin, California, using hydrological simulation program—FORTRAN (HSPF). Water 8 (10), 432.

Stern, M.A., Flint, A.F., Flint, L.E., Alpers, C.N., 2019. Characterization of hydrology and sediment transport following drought and wildfire in Cache Creek, California. California. Submitted for publication.

Swets, D.L., Reed, B.C., Rowland, J.R., Marko, S.E., 1999. A weighted least-squares approach to temporal smoothing of NDVI. In: Proceedings of the 1999 ASPRS Annual Conference, from Image to Information, Portland, Oregon, May 17-21. American Society for Photogrammetry and Remote Sensing, CD-ROM, Bethesda, Maryland, 1 disc.

Tromble, J.M., 1983. Interception of rainfall by tarbush. J. Range Manag. 36, 525–526. https://doi.org/10.2307/3897960.

United States Geological Survey (USGS), National Geospatial-Intelligence Agency (NGA), National Aeronautics and Space Administration (NASA), 2014. Shuttle radar topography mission 1 arc-second global. Available online at: https://earthexplorer.usgs.gov. Accessed 10/10/2017.

U.S. Army Corps of Engineers, 2010. Hydrologic Modeling System HEC-HMS: User's Manual Version 3.5. U.S. Army Corps of Engineers, Institute for Water Resources, Hydrologic Engineering Center, Davis, CA, p. 316.

U.S. Department of Agriculture, Natural Resources Conservation Service, 2009. Small Watershed Hydrology: WinTR-55 U.S.Er Guide. Conservation Engineering Division.

USFS Geospatial Technology, Applications Center, 2018. Frequently asked questions. https://www.fs.fed.us/eng/rsac/baer/barc.html. Accessed 8/16/2018.

van Dijk, A.I.J.M., Bruijnzeel, L.A., 2001. Modeling rainfall interception by vegetation of variable density using an adapted analytical model. Part 1. J. Hydrol. 247, 230.

Wainwright, J., Parsons, A.J., Abrahams, A.D., 1999. Rainfall energy under creosotebush. J. Arid Environ. 43, 111–120. https://doi.org/10.1006/JARE.1999.0540.

Wang, J., Endreny, T.A., Hassett, J.M., 2005. A flexible modeling package for topographically based watershed hydrology. J. Hydrol. 314 (1–4), 78–91.

Wang, J., Endreny, T.A., Nowak, D.J., 2008. Mechanistic simulation of tree effects in an urban water balance model. J. Am. Water Resour. Assoc. 44, 75–85.

Westerling, A., Brown, T., Schoennagel, T., Swetnam, T., Turner, M., Veblen, T., 2014. Briefing: Climate and Wildfire in Western US Forests. USDA Forest Service RMRS-P-71.

Williams, C.J., Pierson, F.B., Robichaud, P.R., Boll, J., 2014. Hydrologic and erosion responses to wildfire along the rangeland–xeric forest continuum in the western US: a review and model of hydrologic vulnerability. Int. J. Wildland Fire 23, 155–172.

Wondzell, S.M., King, J.G., 2003. Post-fire erosional processes in the pacific northwest and Rocky mountain regions. For. Ecol. Manag. 178, 75–87.

Ye, W., Bates, B.C., Viney, N.R., Silvapan, M., Jakeman, A.J., 1997. Performance of conceptual rainfall runoff models in low-yielding ephemeral catchments. Water Resour. Res. 33 (1), 153–166.